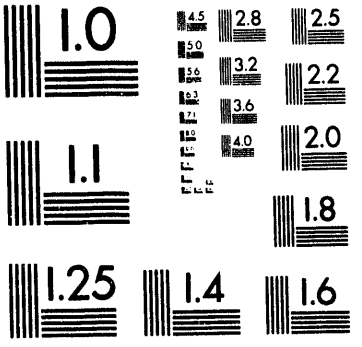
1.0
1.1
1.25
1.4
1.6
1.8
2.0
2.2
2.5
2.8
3.2
3.6
4.0
4.5
5.0
5.6
6.3
7.1

1 of 1

SAND--93-0386C
Conf-9305159--6

Computational Analysis of Debris Formation in SXPL Laser-Plasma Sources

Timothy Trucano, Dennis Grady, Rick Olson, and Archie Farnsworth

Sandia National Laboratories
P. O. Box 5800
Albuquerque, New Mexico 87185

Abstract

One of the goals of soft X-ray projection lithography (SXPL) is to devise laser plasma X-ray sources that minimize or entirely eliminate condensed debris. Our progress in developing a computational methodology for analyzing and predicting the formation of target debris in laser generated soft X-ray sources is presented. Our numerical approach requires (1) simulation of the laser/target interaction using the LASNEX radiation hydrodynamics code; (2) simulation of the thermomechanical response of the target using the CTH strong shock code; (3) and detailed debris predictions from extrapolation of CTH results to millisecond time scales via post-processing techniques. We will discuss scaling issues, give examples of calculations, and discuss experimental data.

Summary of Debris Formation

The compact laser plasma X-ray sources that we are concerned with in this paper have been documented by Kubiak, et al. [3,4]. We will start with an informal discussion of the phenomenology of debris production in such sources.

Briefly, we employ 248 μm KrF laser sources, with pulse durations of approximately 20 to 40 ns FWHM, approximately 100 μm radius spot sizes, and up to 1 Joule pulse energies to yield laser pulse intensities on the order of 10^{11} watts/cm^2. Such pulses are delivered to a variety of metal targets, including tin, gold, tungsten, and tantalum. At intensities of 10^{11} W/cm^2, inverse bremsstrahlung dominates the pulse absorption, which occurs at the critical density ρ_c in a plasma region offset from the solid density region of the target metal. (See Figure 1.) Soft X-rays having peak energies near 300 eV are produced in the maximal absorption region.

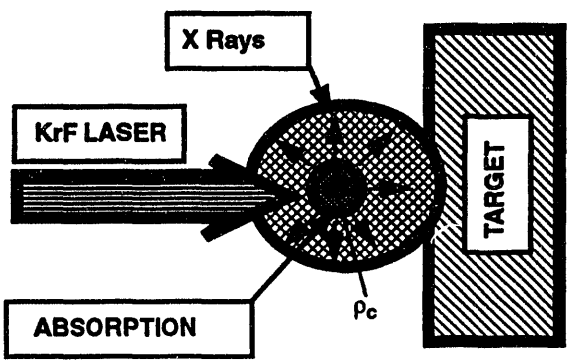

Figure 1. Schematic of laser pulse absorption.

X-ray ablation of the metal target occurs, producing additional plasma and creating a high ablation pressure at the nominal solid density/plasma interface. By this process, kinetic energy is delivered to the solid body of the target. After the completion of the laser pulse, the residual target kinetic energy produces material deformation which is similar to a hypervelocity impact event [5]. A crater is formed, along with a variety of ejecta. Depending on pulse characteristics and material, this ejecta can vary from solid fragments to material occupying thermodynamic states in the mixed liquid/vapor region.

The plasma plume formed during the laser pulse absorption and subsequent ejecta from the condensed target create the debris which complicates the use of these X-ray sources for lithographic applications. By degrading the efficiency of the X-ray optical components that are used to collect, guide, and focus

source X-rays, the lifetime of these components is substantially reduced. The goal is to devise plasma X-ray sources that minimize or entirely eliminate the debris. Many parameters related to target characteristics and laser pulse characteristics are important in any attempt to engineer a solution to the problem of debris production. It is a challenge to understand the details well enough to explain current data and provide analysis tools for designing systems.

In the following section we will discuss the interaction of the pulse and the target in greater detail. Next, we will present a simple result that identifies important scalings relevant to debris production. Then, we will illustrate linked LASNEX/CTH calculations. Finally, we will conclude with a brief discussion of computational debris analysis.

Laser Absorption Simulation

To model target response over times from immediate absorption of the laser pulse (~ 100 nanoseconds duration) to the ejection of solid debris (possibly up to milliseconds) requires the coupling of LASNEX to CTH. The two-dimensional Lagrangian code LASNEX [9] has all of the physics needed to simulate the laser absorption, but it does not model the thermomechanical response of the solid target accurately. While CTH, a one-, two-, and three-dimensional Eulerian code [5], is capable of modeling the solid target behavior correctly, including phase transitions, viscoplastic strength, and fracture, it does not implement laser absorption physics.

LASNEX simulations have been successful in predicting characteristics of the X-ray source region when compared with experimental data [6,8]. This is encouraging because the usual applications of LASNEX to fusion-related laser/target interactions are at larger laser intensities (~ 10^{15} w/cm^2). We feel comfortable in initiating our target response calculations with LASNEX simulations, but we stress that the task of benchmarking the overall thermomechanical response of the target in our simulations remains to be completed.

LASNEX provides an initial state for a subsequent CTH calculation. This initial state is typically near the end of the laser pulse, when essentially all of the pulse energy has been absorbed. A complete thermodynamic and kinematic state of the target is initialized in CTH at this time. Some care must be exercised because LASNEX is a two-temperature code (separate electron and ion temperatures) and includes radiation energy in the total energy budget. CTH is a single temperature (ion) code, with no radiation transport. The link is reasonable by the end of the laser pulse because the electron and ion temperatures have equilibrated in LASNEX, and the amount of radiation energy is quite small. It is our experience that the linked calculations are insensitive to the precise link time as long as "most" or "all" of the laser pulse has been absorbed and we do not link "too long" after the pulse has ended. Otherwise, unphysical LASNEX material motion may occur. (See below.) Linked calculations are sensitive to the zoning used in both codes.

Although LASNEX calculations are necessary precursors to performing linked calculations, useful information is generated by LASNEX independent of subsequent CTH calculations. Quantities of importance for debris modeling that can be extracted from LASNEX include time evolution of the target temperatures, densities, early time material motion, and the ablation pressure field which drives crater evolution and material ejecta.

Two additional caveats underlie our linked calculations. First, plasma thermal conduction effects are not included in CTH in the present discussion. Therefore, residual hot plasma mapped into CTH during the link may not cool as rapidly as it should. This may tend to increase ultimate crater volumes calculated by CTH.

Second, the solid target material motion computed by LASNEX even during the laser pulse may not be entirely correct, due to the absence of solid mechanics effects in the material descriptions. For example, material deformation may be greater than experiments would suggest because of the absence of viscoplastic effects. This might then introduce errors in the CTH initial conditions that ultimately lead to errors in the cratering and ejecta analyses. Overprediction of crater volumes when compared with experiments may occur, but the degree to which this is true needs to be assessed experimentally. Since our major intent is to acquaint the reader with our approach, we will not discuss this further.

Simple Scaling

A simple equation relating the crater volume resulting from a given laser pulse and target characteristics can be derived. Such a relationship is useful for gaining insight into important parameters which influence crater volume. The reason to focus on crater volume is that it is directly proportional to the volume of material removed from the target by a given laser pulse. Therefore, parameter trends observed for the crater volume will also hold true for debris generation.

We make the following assumptions: (1) the laser pulse exerts a constant ablation pressure P_0 on the target material at the base of the crater as the crater develops; (2) P_0 acts for the duration of the pulse τ; (3) the pressure is applied to an area πa^2, where a is the radius

of the laser spot (so we are assuming that the laser spot is circular in the focal plane). Then, we require the pressure applied to the full area of the developing crater to be a simple function of radius r, which is constrained to equal P_0 when r=0, and equal zero when r=a. An appropriate form for this pressure is:

$$P = P_0 \cdot \left[1 - \left(\frac{r}{a}\right)^n\right] \qquad (1)$$

This is depicted below in Figure 2.

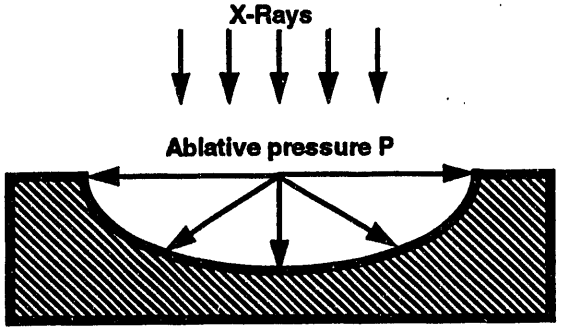

Figure 2. Simple ablation driven crater formation.

Using (1), we may balance the work done on the target metal by the laser pulse through the pressure P and the work needed to form a crater of given volume in a rigid plastic material having yield strength Y. The result that we have derived is an equation for the crater volume in terms of pulse and target parameters:

$$V = \beta \cdot \frac{\tau P_0^2 a^2}{Y \rho U_S} \qquad (2)$$

In (2), V is the crater volume, ρ is the target density, U_S is the wave speed in the target material at the pressure P_0, and β is a constant that depends upon the exponent n in (1).

P_0 can be estimated in a variety of ways. For example, in [7] Pirri shows that

$$P_0 \propto M^{7/18} \cdot \lambda^{-2/9} \cdot I \cdot a^{1/3} \qquad (3)$$

where M is target atomic mass, λ is laser wavelength, and I is the pulse intensity. We can also evaluate P_0 from LASNEX simulations. An illustration of a LASNEX result is shown in Figure 3. There, we see that the ablative pressure is far from constant. This particular data is somewhat noisy, as shown by the signal that appears after the end of the pulse. From such LASNEX data, a mean pressure can be computed and used for P_0.

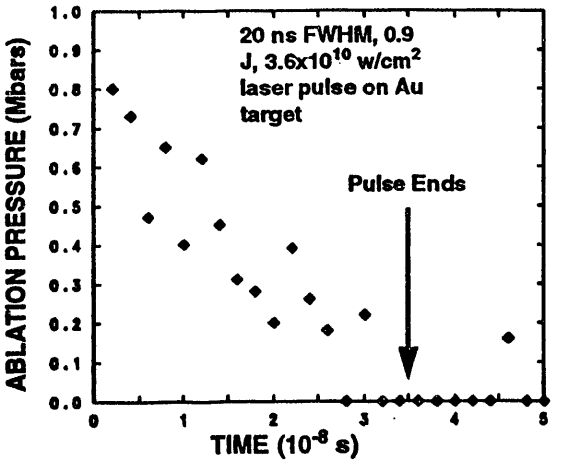

Figure 3. Sample LASNEX ablation pressure.

The simple relationship (2) is very interesting because it suggests that crater volume is more sensitive to laser pulse parameters than to target properties, although the assumed rigid-plastic flow stress Y may mask more complex viscoplastic rate and scale effects. This suggests that laser pulse adjustments can have a "quadratic" effect on crater volume.

For the sake of illustrating (2) further, assume that P_0 = 200 kbars, τ = 34 ns, and a = 75 μm. Then, we compute crater volume from (2) for seven different metals and plot this vs. Y in Figure 4. We have scaled the data by the crater volume for tungsten. On the same plot, we have also presented experimental volume of removed material per laser pulse data from [4]. These data are determined for laser pulses having the same parameters as used to determine the crater volume and are also normalized to the value for tungsten.

As mentioned above, the volume of material removed by a given laser pulse is some fraction of the developed crater volume, and this will depend upon material. Thus, we see significant quantitative differences between the experimental and theoretical data in Figure 4. However, this simple theory is able to predict the trend of the experimental data with variation of target metal for all seven metals. It is our opinion that simple relationships such as (2), and elaborations of them that are more specific to SXPL dynamic loading conditions, can provide real engineering insight into the debris formation process. For example, both experiment and theory in the present discussion suggest that tungsten targets will produce less debris than tin. Quantitative differences in the debris between these two metals, such as fragment sizes or velocity distributions, are not assessed by this simple theory. (2) also suggests

that if the mean ablation pressure could be reduced by a factor of 3, for example, the resulting crater volume would be a factor of nine smaller. The ejecta from the crater would then be decreased by this proportion also, depending on the scaling of ejecta volume with crater volume.

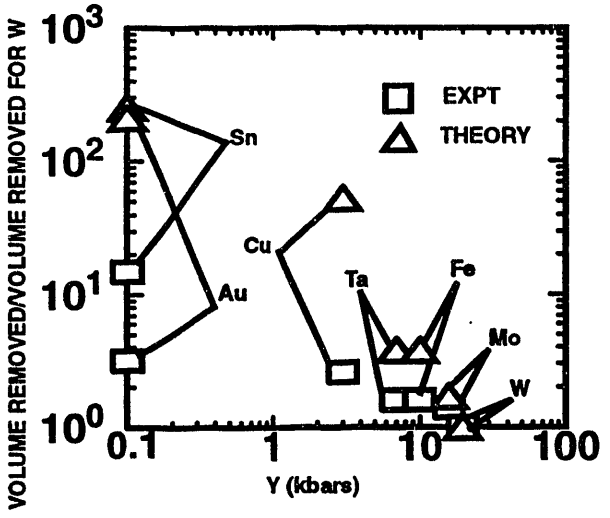

Figure 4. Relative crater volumes and volume of removed material.

Linked Calculations: An Example

Simple relations like (2) are very important for understanding both experimental and computational data. They also underlie more detailed analyses of CTH simulations of the debris ejected during the cratering process, such as velocity and mass distributions of ejecta, and the expected thermodynamic state of the ejecta. We will illustrate linked LASNEX/CTH calculations in this section.

Figure 5 demonstrates the growth of a crater in a gold target produced by a laser pulse having the same characteristics as depicted in Figure 3. The spot size for this particular pulse is 200 μm in diameter (shown in the 50 ns computer snapshot). The link time from LASNEX is 50 ns in this case. The CTH calculation is carried out for 1 μs beyond this time. The growth of the crater can be seen in these pictures, along with the upwelling of material at the edges of the crater. Inspection of the CTH calculation reveals that this material is moving upward at speeds between 50 and 150 m/s in a heterogeneous velocity field. Note that the computed material speeds are compatible with experimental observations of debris velocities in certain experiments [1].

The linked calculations are 2-D, axisymmetric calculations. An on-axis jet of close-to-solid density gold appears by 750 ns in our calculation. This jet is a manifestation of a real physical effect - low density plasma accelerating a high density material is a hydrodynamically unstable material motion. The jet observed in the calculation is a numerical artifact of this, although it is enhanced somewhat by the peculiarities of computed flows near the axis of symmetry. Evidence for the presence of unstable flow is observed in the residual craters of single pulse experiments. These instabilities can contribute to debris production in laser/target interactions, but require further study.

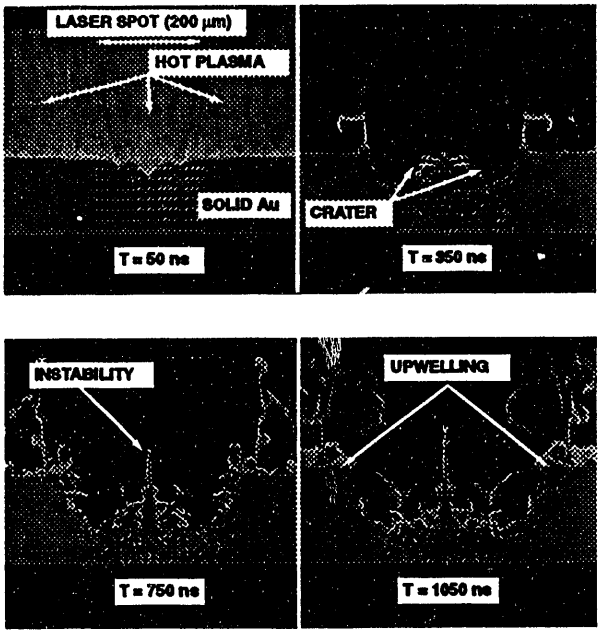

Figure 5. Crater evolution in gold.

Calculations such as that seen in Figure 5 are very sensitive to changes in laser pulse parameters and target material properties. The calculations support the general trends found in our previous analysis. As an illustration, for a given laser pulse the computed crater in tungsten is much smaller than in copper, which is, in turn, smaller than in gold. We have also found that computed crater volumes qualitatively obey the scaling stated in (2) (increase strongly with intensity and laser spot size, less strongly with laser pulse duration). Details of the calculations, such as the instability features, speeds of the upwelling material near the crater edges, and the thermodynamic state of the incipient ejecta also change with laser pulse parameters and target material.

Predicting Debris Characteristics

By using techniques similar to those discussed in [2], a detailed prediction of ejecta characteristics by CTH calculations can be performed. In this approach, the

heterogenous kinematic and mechanical states of the material near the edges of the crater are used as inputs for *final-state dynamic fragmentation theories*. In such theories, it is assumed that a good approximation to the breakup of the target material is found by applying frozen-time fracture criteria (which may be quite complex) to the final computed state of the material. These criteria can be statistical and can yield predictions of ejecta size, mass, and velocity distributions which can be compared with experimental data. The final-state fracture criteria can be applied on small spatial scales, ultimately limited only by the scale of the computational mesh.

Thus, full coupling of the fragmentation process to the numerical material flow is neglected. This approximation is not valid in all cases, but it has proven to be reasonable for a variety of applications, including impact events. We note that a fully coupled approach using a continuum physics code has some philosophical difficulties because of questions concerning the destruction of the continuum by the fragmentation process.

We illustrate this technique with a simple example. As discussed in [2], material fragmentation results from a dynamic load when the energy needed to fracture material, measured by a *surface energy* γ, is balanced by the energy available for creating fragments. This latter quantity can be approximated by the kinetic energy of expansion of material. For a dynamic load given by the pressure in (1), and with n=2, the following expression for mean fragment size of the material can be derived:

$$S = \left(\frac{12 \cdot \gamma \cdot a^4 \cdot \rho}{P_0^2 \cdot \tau^2} \right)^{-1/3} \qquad (4)$$

Equation (4) suggests scaling behavior that could be compared with experimental data. We note here that for laser pulse characteristics similar to those used in Figure 4, equation (4) predicts mean fragment sizes for target materials of interest to SXPL on the order of one to four microns. These sizes have been observed in experiments [1]. Note that surface energy γ is difficult to determine experimentally for metals at SXPL conditions (in the liquid/vapor coexistence region). We used values between 0.5 and 3.0 J/m^2, but further work is required to determine γ more accurately for hot metals.

Acknowledgments

This work performed at Sandia National Laboratories supported by the U. S. Department of Energy under contract number DE-AC04-76DP00789.

References

1. H. A. Bender, A. M. Eligon, A. Hanzo, and W. T. Silfvast, "Velocity Characterization of Target Debris From a Laser-Produced Plasma Utilizing a "time-of-flight" technique," in OSA Proceedings on Soft X-Ray Projection Lithography, Vol. 18, (1993-to be published).

2. D. E. Grady and M. E. Kipp, "Fragmentation of Solids Under Dynamic Loading," in Structural Failure, John Wiley & Sons (1989).

3. G. D. Kubiak, et al, "Diffraction-Limited Soft X-Ray Projection Lithography With a Laser Plasma Source," J. Vac. Sci. Technol. B9, 3184 (1991).

4. G. D. Kubiak, K. W. Berger, and S. J. Haney, "Laser Plasma Source Targets for SXPL: Production and Mitigation of Debris," in OSA Proceedings on Soft X-Ray Projection Lithography, Vol. 18, (1993-to be published).

5. J. M. McGlaun, S. L. Thompson, and M. G. Elrick, "CTH: A Three-Dimensional Shock-Wave Physics Code," Int. J. Impact Engng., 10, 351 (1990).

6. R. E. Olson, "Computational Simulations of a SXPL Laser Plasma Source," in OSA Proceedings on Soft X-Ray Projection Lithography, Vol. 18, (1993-to be published)

7. A. N. Pirri, "Theory for Laser Simulation of Hypervelocity Impact," Phys. Fluids, 20, 221 (1977).

8. P. D. Rockett, J. A. Hunter, and R. E. Olson, "XUV Conversion Efficiency in a Low Intensity KrF Laser-Plasma For Projection Lithography," OSA Proceedings on Soft X-Ray Projection Lithography, Vol. 12 (1991).

9. G. Zimmerman and W. Kruer, "Numerical Solution of Laser-Initiated Fusion," Comm. Plasma Phys., 2, 85 (1975).

DATE
FILMED
10/20/93
END